

Asymmetric Fano resonance and bistability for high extinction ratio, large modulation depth, and low power switching

Landobasa Y. Mario, S. Darmawan, and Mee K. Chin*

Photonics Research Center, School of Electrical and Electronic Engineering
Nanyang Technological University, Singapore 639798.

*emkchin@ntu.edu.sg

Abstract: We propose a two-ring resonator configuration that can provide optical switching with high extinction ratio (ER), large modulation depth (MD) and low switching threshold, and compare it with two other conventional one-ring configurations. The achievable input threshold is $n_2 I_{IN} \sim 10^{-5}$, while maintaining a large ER ($> 10\text{dB}$) and MD (~ 1) over a 10-GHz (0.1 nm) optical bandwidth. This performance can also be achieved by the ring-enhanced Mach-Zehnder interferometer, and is one to two orders of magnitude better than the simple bus-coupled one-ring structures, because of the use of asymmetric Fano resonance as opposed to the usual symmetric resonance of a single ring. The sharpness and the asymmetry of the Fano resonance are linked to the low switching threshold and the high extinction ratio, respectively, and also accounts for the different dependence on ring dimensions between the one- and two-ring structures.

© 2006 Optical Society of America

OCIS codes: (130.3120) Integrated Optic Devices; (230.5750) Resonators; (130.2790) Guided waves; (190.1450) Bistability

References and Links

1. B.E. Little, S. T. Chu, P. P. Absil, J. V. Hryniewicz, F. G. Johnson, F. Seifert, D. Gill, V. Van, O. King, and M. Trakalo, "Very high-order microring resonator filters for WDM applications," *IEEE Photon. Technol. Lett.* **16**, 2263-2265 (2004).
2. T. A. Ibrahim, R. Grover, L. -C. Kuo, S. Kanakaraju, L. C. Calhoun, P. -T. Ho, "All-optical AND/NAND logic gates using semiconductor microresonators," *IEEE Photon. Technol. Lett.* **15**, 1422-1424 (2003).
3. J. Niehusmann, A. Vörckel, P. H. Bolivar, T. Wahlbrink, W. Henschel, and H. Kurz, "Ultrahigh-quality-factor silicon-on-insulator microring resonator", *Opt. Lett.* **29**, 2861-2863 (2004).
4. D. A. B. Miller, "Refractive Fabry-Perot Bistability with Linear Absorption: Theory of Operation and Cavity optimization," *IEEE J. Quantum Electron.* **17**, 306-311 (1981).
5. F. Sanchez, "Optical bistability in a 2x2 coupler fiber ring resonator: parametric formulation," *Opt. Commun.* **142**, 211 (1997).
6. Y. Dumeige, D. Arnaud, P. Feron, "Combining FDTD with coupled mode theories for bistability in micro-ring resonators," *Opt. Commun.* **250** (2005) 376-383.
7. Y. Dumeige, P. Feron, "Dispersive tristability in microring resonator," *Phys. Rev. E*, **72** 066609 (2005).
8. J. Danckaert, K. Fobelets, I. Veretennicoff, "Dispersive optical bistability in stratified structures," *Phys. Rev. B*, **44**, 15, 8214 (1991).
9. B. Maes, P. Bienstman, R. Baets, "Switching in coupled nonlinear photonic crystal resonators," *J. Opt. Soc. Am. B* **22**(8), 1778-1784 (2005).
10. V. R. Almeida and M. Lipson, "Optical bistability on a silicon chip," *Opt. Lett.* **29**, 2387-2389 (2004).
11. S. Fan, W. Suh, and J. D. Joannopoulos, "Temporal coupled-mode theory for the Fano resonance in optical resonators," *J. Opt. Soc. Am. A*, **20**(3), 569-572 (2003).
12. Y. Lu, J. Yao, X. Li, and P. Wang, "Tunable asymmetrical Fano resonance and bistability in a microcavity-resonator-coupled Mach Zehnder Interferometer," *Opt. Lett.* **30**, 3069-3071 (2005).
13. L. B. Maleki, A. B. Matsko, A. A. Savchenkov, and V. S. Ilchenko, "Tunable delay line with interacting whispering-gallery-mode resonator," *Opt. Lett.* **29**, 626 (2004).
14. I. Chremmos, and N. Uzunoglu, "Reflective properties of double-ring resonator system coupled to a waveguide," *IEEE Photon. Technol. Lett.* **17**, 2110-2112, 2005
15. Y. M. Landobasa, S. Darmawan, and M. K. Chin, "Matrix Analysis of 2-D Micro-resonator Lattice Optical Filters," *IEEE J. Quantum Electronics* **41**, 1410-1418 (2005).

16. A. Yariv, "Critical coupling and its control in optical waveguide-resonator systems," *IEEE Photon. Technol. Lett.* **14**, 483-485, 2002.
17. A.R. Cowan and J.F. Young, "Optical bistability involving photonic crystal microcavities and Fano line shapes," *Phys. Rev. E* **68** 046606 (2003)
18. V. Van, T. A. Ibrahim, P.P. Absil, F. G. Johnson, R. Grover, and P-T. Ho, "Optical signal processing using nonlinear semiconductor microring resonators," *IEEE J. Quantum Electron.* **8**, 705-713 (2002).
19. B. L. Lawrence, M. Cha, W. E. Torruellas, G. I. Stegeman, S. Etemad, G. Baker, F. Kajzar, "Measurement of the complex nonlinear refractive index of single crystal p-toluene sulfonate at 1064 nm," *Appl. Phys. Lett.* **64** (1994), 2773.
20. C. Y. Chao and L. J. Guo, "Reduction of surface scattering loss in polymer mirroring using thermal-reflow technique," *IEEE Photon. Technol. Lett.* **16**, 1498-1500 (2004).
21. M. Notomi, A. Shinya, S. Mitsugi, G. Kira, E. Kuramochi, and T. Tanabe, "Optical bistable switching action of Si high-Q photonic-crystal nanocavities," *Opt. Express* **13**, 2678-2687 (2005).
<http://www.opticsinfobase.org/abstract.cfm?URI=oe-13-7-2678>

1. Introduction

In integrated optics, ring resonator is a good candidate for realizing many useful devices such as modulator, switch, active/passive filter, and multiplexer, especially when recent fabricated ring resonators have reasonably high Q factor ($\sim 10^4$) and low loss [1-3]. This high-Q cavity is of considerable interest, particularly in all-optical switching when combined with nonlinearity [4]. Bistability and multistability have been demonstrated in various configurations, i.e. the ring resonator coupled to one or two bus waveguides [5-6], the ring resonator arrays [7], Bragg gratings [8], and photonic bandgap cavities [9]. A good optical switch is characterized by low input threshold power, high extinction ratio (i.e. >10 dB), high modulation depth, and reasonable optical bandwidth. The extinction ratio (ER) is defined as the ratio between the logic "1" and "0", the modulation (MD) is defined as the difference between the logical "1" and "0" normalized by the incident power, and the optical bandwidth is defined as the signal wavelength tolerance for a given ER. While low threshold has been achieved using cavity-enhanced nonlinear response, the demonstrated extinction ratio and modulation depth are usually very low (as an example, for the first Silicon ring resonator switch using thermal nonlinearity [10], MD ~ 0.3 and ER = 3 dB, according to our definitions). There is thus a need to search for the optimal switch configurations with significantly better performance.

In this paper we show that the extinction ratio and modulation depth are determined by the shape of the resonance while the switching power is dependent on its sharpness. It is difficult to achieve both high ER and large MD for a single-ring with a symmetric resonance. On the other hand, they can both be significantly enhanced by using an asymmetric Fano resonance [11]. Such a Fano resonance can be generated by the conventional ring-enhanced MZI (REMZI) where the resonator is coupled to a Mach-Zehnder interferometer [12]. Alternatively, it can be generated, with more flexibility, by using a new and novel two-ring configuration we propose here. The present two-ring configuration is different from other reported two-ring structures [13-14], as it is designed to harness the narrow and asymmetric lineshape of the Fano resonance to achieve optimal switching performance. We show that both configurations can achieve optical switching with very low threshold ($n_2 I_{IN} \sim 10^{-6}$), high extinction ratio (> 30 dB) and large modulation depth (~ 1). We also consider their sensitivity to wavelength and show that a larger optical bandwidth can be obtained but at the expense of switching threshold.

In section 2 we discuss bistability in the conventional bus-coupled one-ring structures using the parametric approach. In section 3 we introduce the Fano resonance through the ring-enhanced MZI and consider its switching performance. This work complements and improves on that reported in [12]. Finally, in section 4 we discuss the new two-ring switching configuration in great detail, culminating in a comparison between the one- and two-ring structures.

2. Bistability in a one-ring configuration

A single ring can be coupled with one or two bus waveguides. Although the operation is different between these two cases, the result as an optical switch is similar, hence for simplicity we consider only the one-bus case below.

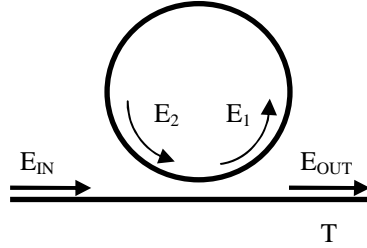


Fig. 1. Schematic of a ring resonator coupled to one bus waveguide.

A lossless single waveguide ring resonator coupled with a bus waveguide, as shown in Fig. 1(a), is an all-pass filter, but in the presence of loss exhibits a resonant transmission profile given by [15]

$$T = \left| \frac{E_{OUT}}{E_{IN}} \right|^2 = \frac{a^2 - 2ra \cos \delta + r^2}{1 - 2ra \cos \delta + r^2 a^2} \quad (1)$$

where δ is the round trip phase, $a = \exp(-\alpha L_c/2)$ is the round-trip amplitude for a cavity with length L_c and linear loss coefficient α , and r is the “reflectivity” of the coupler which is related to the coupling coefficient or “transmittivity” (t) by $r = \sqrt{1-t^2}$. The transmission is symmetric and minimum on resonance when $\delta = 2m\pi$ (m is an integer). On resonance, the transmission is zero when $r = a$, a condition known as *critical coupling* [16]. In the case where the ring is a Kerr medium with nonlinear coefficient n_2 , the round-trip phase is the sum of a linear part and a nonlinear part:

$$\delta = \delta_L + \delta_{NL} = k_0 (n_{\text{eff}} + n_2 I_R \eta) L_c \quad (2)$$

where $k_0 = 2\pi/\lambda$, n_{eff} is the waveguide effective index, $\eta = (1 - e^{-\alpha L_c})/\alpha L_c$ is the length reduction factor which accounts for the power loss in the ring, and I_R is the maximum intensity in the ring. Inside the ring, the optical power will build up such that the build-up factor I_R/I_{IN} is given by

$$\frac{I_R}{I_{IN}} = \frac{1 - r^2}{1 - 2ra \cos \delta + r^2 a^2} \equiv B \quad (3)$$

where I_{IN} is the input intensity to the bus waveguide. We have assumed that the nonlinear absorption is small compared with the nonlinear refraction, as is usually done [4]. By incorporating Eq. (3) in Eq. (2) one achieves a mapping between δ and I_{IN} , and consequently with Eq. (1), the transmission can be plotted as a function of I_{IN} . This approach is analogous to the parametric formulation [6]. It can be seen that near resonance where $\cos \delta \sim 1 - \delta^2$, Eq. (3) is a cubic equation in I_R , and hence, for a suitable value of I_{IN} , there can exist three real solutions.

Some examples are shown in Fig. 2(a) for several wavelengths below the resonance (the resonance is at $\lambda = 1568$ nm), all under the critical coupling condition ($r = a$). These examples are for the case where n_2 is negative, as is the case for polymers [19]. The operating wavelengths are all below the resonance wavelength. Note that the transmission shows

bistability behavior only at some wavelengths, but not all (e.g., no bistability exists at 1567.8nm). As pointed out by Miller [4], for bistability to occur there is a minimum critical detuning required, given by $\omega - \omega_0 = \Delta\omega_{FWHM} \sqrt{3}/2$, where ω_0 is the resonance frequency and $\Delta\omega_{FWHM}$ is the FWHM linewidth of the resonator. The critical detuning is the point where the build-up resonant function (Eq. (3)) has the maximum slope. If this requirement is met, then bistability occurs as the incident power is increased because of the nonlinear shift of the resonance towards λ , causing the intra-cavity power to build up, which in turn hastens the shift, leading to an unstable situation. This positive feedback increases the slope of the leading edge of the transmission spectrum relative to the linear case [17]. At some critical power the slope can change sign, giving rise to two possible transmission values at the same wavelength. Hence, the transmission falls abruptly to the lower value on the other side of the resonance where the condition is stable (i.e., where increase in I_{IN} reduces the build-up factor). This is the *turn-off* point indicated by the down arrow.

Similarly, a reduction in power from this point will lead to an upward transition at the *turn-on* point. Note that the minimum transmission is zero only under critical coupling. The ON/OFF ratio at the turn-off point is generally smaller than that at turn-on, and determines the extinction ratio (ER) of the switch if the power is held here in the OFF state. Hence, to maximize the ER and modulation depth, it is important to minimize the off-state transmission *at* the turn-off point, while maximizing the on-state transmission at the initial detuning. To align the minimum transmission point closer to the turn-off point, one way is to operate very close to the critical detuning, but the problem with this is that the ON transmission amplitude is also substantially reduced (hence the modulation depth is small), and the difference between the turn-on and turn-off powers becomes very small. Similar effect may be achieved by increasing the round-trip loss, as shown in Fig. 2(b). This is because increasing the loss broadens the resonance and increases the critical detuning, which has the same effect as having the operating wavelength closer to critical detuning. However, the broadened linewidth increases the switching threshold, as expected because of the smaller build-up factor. To maximize the build-up factor at the given loss, one must further satisfy the critical coupling condition $r = a$. Under this condition the achievable input threshold is in the order $n_2 I_{IN} \sim 10^{-4}$.

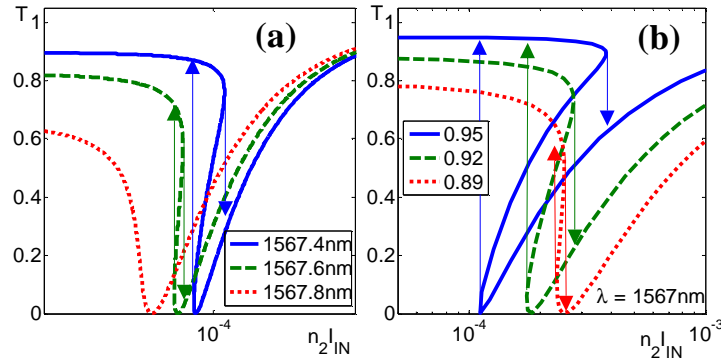


Fig. 2. The transmission as a function of incident power for a critically coupled ring for (a) $r = 0.95$ for various near-resonant wavelengths, and (b) at a fixed wavelength, $\lambda = 1567$ nm, for various losses under the critical coupling condition.

3. Ring-enhanced Mach-Zehnder Interferometer

We have seen that in the simple one-ring case, it is not possible to achieve simultaneously high extinction ratio and large modulation depth. This is fundamentally because of the symmetric shape of the resonance which gives rise to the general behavior seen in Fig. 2. To achieve a high ER one has to operate very close to critical detuning and inevitably the linear transmission amplitude will drop leading to limited modulation depth. To maximize the ER and MD simultaneously, one would need to engineer the minimum turning point of the

transmission curve to be directly below the turn-off point without depressing the ON transmission level. Such a situation can be achieved by using an *asymmetric* resonance such as the Fano resonance. Fano resonance is a result of interference between two pathways [11]. One way to generate a Fano resonance is by the use of a ring resonator coupled to one arm of a Mach-Zehnder interferometer, with a static bias in the other arm, as shown in Fig. 3.

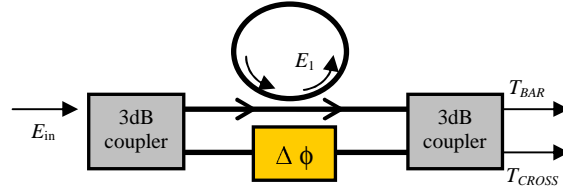


Fig. 3. Schematic of a REMZI with phase bias $\Delta\phi$.

The outputs of such a ring-enhanced MZI (REMZI) depend on the interference between the frequency-sensitive phase response of the ring resonator and the static phase bias. Interference between the direct and indirect paths only takes place when the ring is near resonance. To maximize the interference the power division in the upper and lower arms is kept equal and the ring is designed with low loss and far from the critical coupling ($r = a$). Under this condition, the outputs at the two arms are given approximately by $T_{\text{BAR}} = \sin^2(\varphi - \Delta\phi)/2$, $T_{\text{CROSS}} = \cos^2(\varphi - \Delta\phi)/2$, where

$$\varphi = \pi - \delta - \tan^{-1} \left\{ \frac{r \sin \delta}{a - r \cos \delta} \right\} - \tan^{-1} \left\{ \frac{ar \sin \delta}{1 - ar \cos \delta} \right\} \quad (4)$$

The phase bias can be used to tune the asymmetry of the resonance, as seen in Fig. 4 which shows the cross port transmission, T_{CROSS} , near resonance. The resonance is very sharp as we have assumed $r = 0.95$. A large r is desirable as a sharp resonance minimizes the switching threshold. When the phase bias is zero, the output is a symmetric function of δ . As $\Delta\phi$ is increased, the asymmetry increases and the Fano resonance shifts slightly to the left. In the lossless case ($a = 1$), by expanding Eq. (4) it can be shown that the shift of the minimum transmission point (where $T_{\text{CROSS}} = 0$) is approximately given by $\delta_{\text{MIN}} = -\Delta\phi(1-r)/(1+r)$, i.e., the shift is *reduced*, relative to the phase bias, by the maximum build-up factor in the ring. Far away from resonance, the transmission approaches asymptotically the value given by $\cos^2(\Delta\phi/2)$.

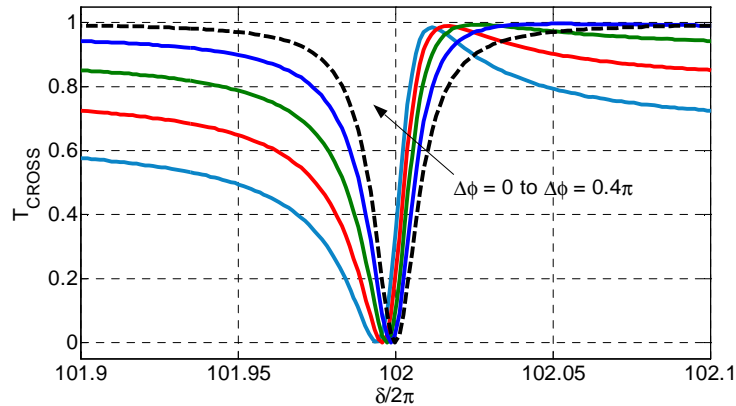


Fig. 4. The Fano resonances for various values of $\Delta\phi$.

Since the Fano resonance curves in Fig. 4 are plotted as a function of total phase $\delta = \delta_L + \delta_{NL}$, where δ_{NL} depends on the intensity, they indirectly trace the transmission as a function of intensity for a particular initial detuning (i.e., operating wavelength). For a material with negative n_2 , the intensity increases from right to left. The intra-cavity intensity is related to the incident intensity by the same build-up factor given in Eq. (3). Therefore, following similar approach as for the one-ring configuration, one can plot the transmission as a function of the input intensity. Some examples are shown in Fig. 5, where the set of colored curves correspond to the set of $\Delta\phi$ values in Fig. 4. Note that by operating very close to the resonance, the initial transmission at low intensity is high. At the same time, $\Delta\phi$ can be used to tune the minimum transmission to align with the turn-off point to achieve the maximum ER. The maximum ER can be as high as 30dB, which is much larger compared with that achievable with a symmetric resonance ($\Delta\phi = 0$). On the other hand, varying $\Delta\phi$ does not change the switching power (as shown in the inset) as I_{IN} does not depend on $\Delta\phi$ [see Eq. (3)]. The switching threshold is of the order of 10^{-5} because of the extremely narrow Fano resonance.

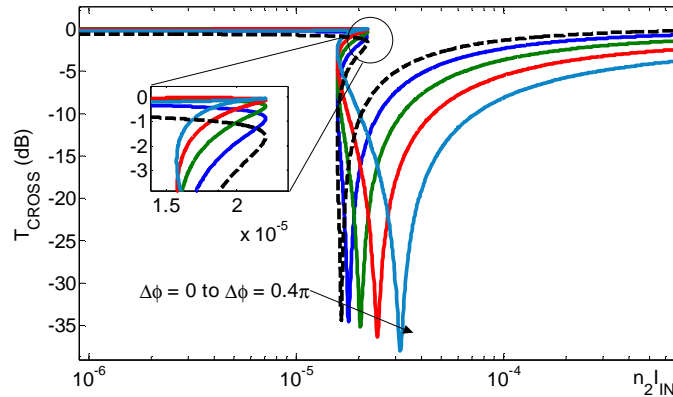


Fig. 5. The Cross output transmission as a function of incident power for various phase biases. The inset shows a blow-up of the curves at the switch-off points.

Because of the narrow resonance, the ER is also very sensitive to wavelength, hence limiting the device's optical bandwidth. As a tradeoff between ER and bandwidth, it may be necessary to compromise the linewidth of the Fano resonance. Figure 6 shows that an ER higher than 10dB can be achieved within a 20GHz ($\Delta\lambda = 0.2\text{nm}$) optical bandwidth.

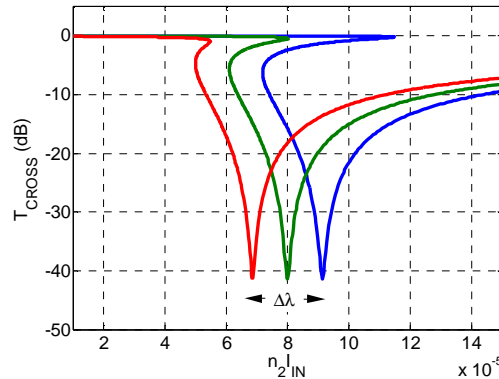


Fig. 6. The achievable bandwidth can be up to 20GHz for relatively high ER. The highest ER can be as much as 40dB, with phase bias $\Delta\phi = 0.2\pi$ and $r = 0.9$.

4. The Two-ring Configuration

A narrow asymmetric Fano resonance can also be generated in the two-resonator configuration shown in Fig. 7. In this case, one path is formed by the lower ring (ring 1) while the other involves the light propagating through the upper ring (ring 2). Fano resonance arises from the interference between the resonant modes in the two ring cavities. Note that the two rings can have different radii, and hence different resonance frequencies. Consequently, the position of the Fano resonance can be tuned by adjusting the relative position of one ring resonance to the other. The detunability of the Fano resonance distinguishes it from that of REMZI. Similarly, the coupling between the bus waveguide and the ring, denoted r_1 , and that between the two rings, r_2 , may be different, and this variability can be used to optimize the asymmetry of the Fano resonance to achieve maximum ER, just as $\Delta\phi$ does in the case of REMZI. As a four-port device, there are two possible output ports, denoted as “drop” (D) and “through” (T), respectively, and the switch can function in a pump and probe configuration [18].

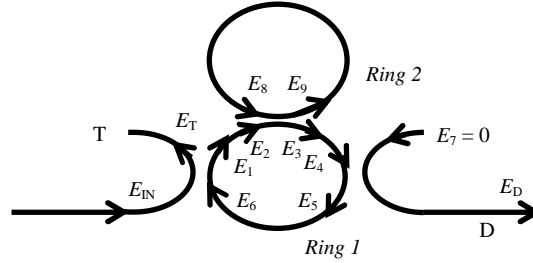


Fig. 7. The two ring resonator configuration with “through” (T) and “drop” (D) outputs. The fields at various points in the structure are indicated.

Intuitively, we expect the linear transmission of the two-ring structure to be similar to that of a single ring coupled with two bus waveguides [14], but “loaded” with the second ring. It is easy to show that the “through” and “drop” transmissions are given by $T = |t|^2$, and $D = |d|^2$, where

$$t = E_T / E_{IN} = r_1 [1 - a_1 T_2 \exp(-i\delta_1)] / [1 - a_1 r_1^2 T_2 \exp(-i\delta_1)] \quad (5)$$

$$d = E_D / E_{IN} = -t_1^2 \sqrt{a_1} T_2 \exp(-i\delta_1/2) / [1 - a_1 r_1^2 T_2 \exp(-i\delta_1)] \quad (6)$$

and $T_2 = E_3 / E_2 = [r_2 - a_2 \exp(-i\delta_2)] / [1 - a_2 r_2 \exp(-i\delta_2)]$ is the factor that incorporates the feedback and interference effect from the upper ring. Note that T_2 is the same as the transmittivity for a single ring coupled to one bus [cf. Eq. (1)]. The coupling between the two resonators causes a splitting of the ring resonance. If the rings are slightly different then the splitting will be asymmetric. This can be shown as follows.

The effect of the upper ring can be represented as an additional loss and a resonant phase perturbation, i.e., $T_2 = |T_2| \exp(i\phi)$, and Eq. (5) may be written as

$$t = r_1 \left(\frac{1 - a \exp(i\delta)}{1 - a r_1^2 \exp(i\delta)} \right) \quad (7)$$

where $a = a_1 |T_2|$, and

$$\delta = \tan^{-1} \left\{ \frac{a_2 \sin(\gamma\delta_1)}{r_2 - a_2 \cos(\gamma\delta_1)} \right\} - \tan^{-1} \left\{ \frac{a_2 r_2 \sin(\gamma\delta_1)}{1 - a_2 r_2 \cos(\gamma\delta_1)} \right\} - \delta_1 \quad (8)$$

The new resonance condition for the two-ring structure is therefore given by $\delta = 2m\pi$. The first two terms in δ represent the loading effect of the upper ring, for which the linear round

trip phase is written as $\delta_2 = \gamma\delta_1$, where γ is the ratio of the linear round-trip phases in the two rings. Eq. (8) is plotted in Fig. 8(a) as a function of δ_1 for two values of γ , and Fig. 8(b) shows the resulting resonance splitting in the T spectra. In the T spectra the resonances appear as minima. Similar to a single-bus ring, the upper ring exhibits a nonlinear 2π phase shift centered at resonance ($\delta_2 = 2\pi m$). When the upper ring is off-resonance, the loading phase is zero meaning that it has no effect on the lower ring, hence the lower ring behaves as a simple dual-bus ring, giving a maximum T when the ring is off-resonance (i.e., δ_1 is an odd multiple of π). However, when the upper ring is on resonance, the nonlinear phase loading kicks in and the loaded lower ring becomes resonant when δ is an even multiple of π . This occurs at two points, giving rise to the two minima in T. When $\gamma = 1$, the two resonances occur on the linear part of the phase hence they are symmetric. When $\gamma \neq 1$ one of the resonances occurs near the nonlinear part of the phase and becomes the asymmetric Fano resonance. The two minima are shifted unequally when γ departs from 1.

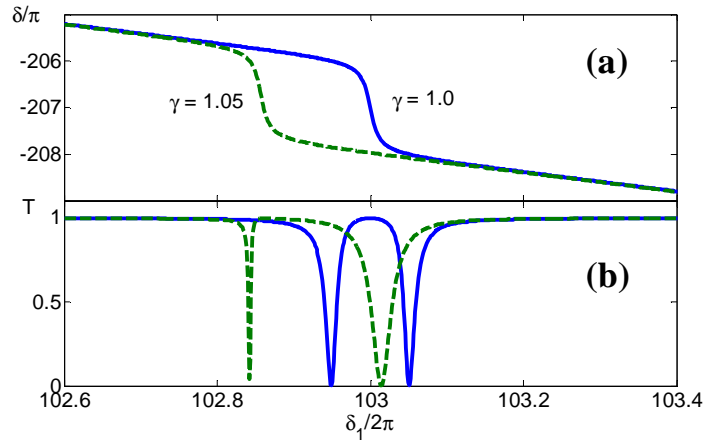


Fig. 8. (a) Plot of Eq. 8 for two different γ values. The nonlinear region is due to the upper ring. (b) The resultant shifts and shape changes in the resonances as γ deviates from 1. For this calculation, we set a_1 and a_2 to be 1 and $r_{1,2} = 0.95$.

Using the finite-difference time domain method we calculated the field distributions corresponding to each resonance for three different values of γ , as shown in Fig. 9. For $\gamma = 1$ the field is confined equally in both rings. However, closer inspection shows that the lower frequency resonance has a symmetric field profile at the coupling point, while the higher frequency resonance has an antisymmetric profile. As γ is increased (decreased), the split resonances shift asymmetrically to the right (left). The sharp, faster-shifting, asymmetric resonance originates primarily from the upper ring (as shown by the field distribution), while the broader resonance is associated mainly with the bottom ring. We shall refer to the sharp asymmetric resonance as the Fano resonance as it is induced by the strong effect of the upper ring, and the broader resonance as the main resonance associated with the lower ring.

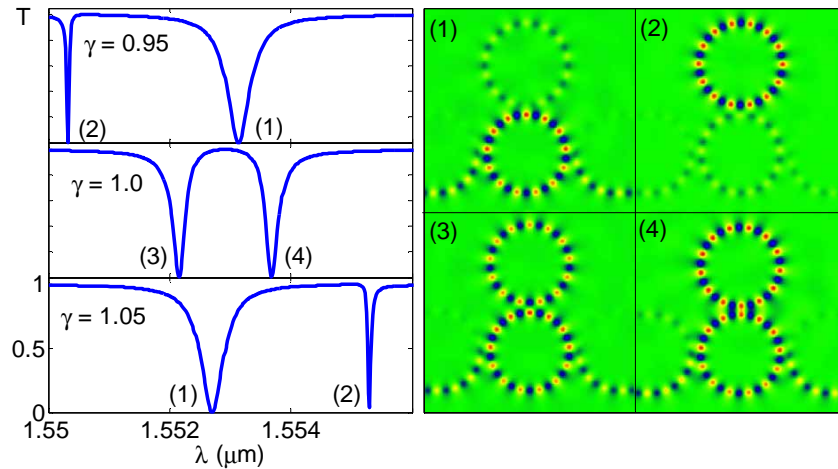


Fig. 9. The analytically calculated “Through” spectra of a linear two-ring structure for different γ values ($r_{1,2} = 0.95$). The right panel shows the associated field distribution for each resonance calculated by FDTD.

In addition to varying the γ , the asymmetry of the Fano resonance can be further tuned by varying the linewidth of the main resonance which depends on r_1 . This is more evident in the D spectra, as shown in Fig. 10. When r_1 is reduced the Fano resonance becomes more asymmetric. Note that while the right edges of the Fano resonances follow the envelope of the main resonance, the steepness on the left edges is relatively stable due to the proximity of the minimum in D, which location is independent of r_1 . The amplitude at the dip changes somewhat for different r_1 but remains small. By operating at a wavelength just before the “dip”, it is possible to achieve switching with high extinction ratio, large modulation depth and low threshold power, as shown below.

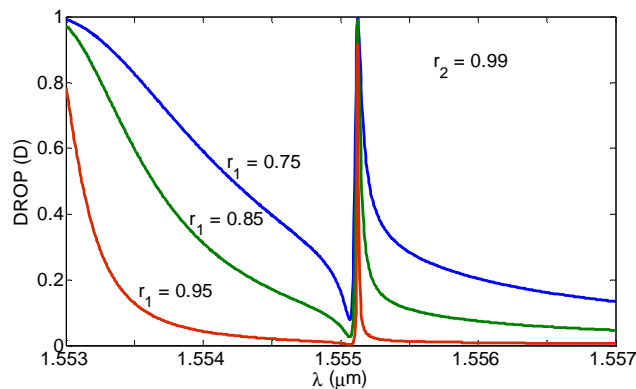


Fig. 10. Fano resonances in the “Drop” spectra with different asymmetries can be obtained by adjusting r_1 , with $\gamma = 1.05$ and $r_2 = 0.99$.

The nonlinear transmission is calculated using the parametric approach [6]. In this approach, the fields in various parts of the structure are expressed in terms of a single parametric field in the upper ring, which in this case is chosen as E_9 . The set of equations required to solve the drop and through amplitudes are

$$\begin{aligned}
E_D &= it_1 T_2 a_1^{1/2} \exp(i\gamma_{NL}^{14} |E_1|^2) \exp(-i\delta_1/2) E_1 \\
E_T &= [1 - a_1 T_2 \exp(-i\delta_1) \exp(i\gamma_{NL}^{16} |E_1|^2)] (r_1 / it_1) E_1 \\
E_{IN} &= [1 - a_1 r_1^2 T_2 \exp(-i\delta_1) \exp(i\gamma_{NL}^{16} |E_1|^2)] (1 / it_1) E_1 \\
E_3 &= [r_2 - a_2 \exp(-i\delta_2) \exp(i\gamma_{NL}^{98} |E_9|^2)] E_9 / it_2 \\
E_2 &= [1 - a_2 r_2 \exp(-i\delta_2) \exp(i\gamma_{NL}^{98} |E_9|^2)] E_9 / it_2 \\
|E_2|^2 a_1^{-1/2} &= |E_1|^2, T_2 = E_3 / E_2, a_{1,2} = \exp(-\alpha_{1,2} L_{1,2} / 2)
\end{aligned} \tag{9}$$

where $\gamma_{NL}^m = k_0 n_{\text{eff}} n_2 c \epsilon_0 [1 - \exp(-\alpha L_m)] / (2\alpha)$ and $\gamma_{NL}^m |E_i|^2$ is the cumulative nonlinear phase over the path L_m from point m to point n . In the linear case, γ_{NL} is set to zero. It can be seen that by fixing E_9 , we can obtain E_2 and E_3 , and thus T_2 , which contains the phase perturbation due to the upper ring. From $|E_2|^2$ we get $|E_1|^2$, which leads to the Through ($T = |E_T/E_{IN}|^2$) and the Drop ($D = |E_D/E_{IN}|^2$) transmission. To calculate the nonlinear response, the wavelength is fixed while E_9 is varied from 0 to ∞ . The nonlinear response is sensitive to wavelength, and bistability exists only for certain wavelengths which depend on the other design parameters (γ , r_1 and r_2). In the following, we assume that the lower ring has a fixed radius of $15\mu\text{m}$.

Figure 11 shows several examples of T as a function of $n_2 I_{IN}$ for the asymmetric case ($\gamma = 1.05$). In (a) we show the dependence on wavelength, with $r_{1,2} = 0.85$ and $a_{1,2} = 0.99$. Bistability exists for the two curves on the right. It can be seen that the ER is greater than 10 dB even if the wavelength changes by 0.1 nm. With careful wavelength tuning, an ER of 20 dB can be achieved. In (b), we show the dependence on asymmetry. We make r_1 and r_2 different so that the Fano resonance becomes more asymmetric (other parameters are $\lambda = 1555$ nm and $a = 0.999$). It is evident that the more asymmetric Fano resonance ($r_1 \neq r_2$) gives a much larger extinction ratio compared with the case where $r_1 = r_2$. In fact, the latter is similar to the one-ring case shown in Fig. 2(b). We further note that the extinction ratio generally decreases when r approaches a . In fact, the dotted curve shows that under the critical coupling condition (when $r_2 = a$), bistability disappears as power is entirely absorbed in the upper ring resonance and the Fano interaction between the two rings is quenched. Hence, critical coupling is undesirable for the two-ring configuration, unlike in the single-ring case.

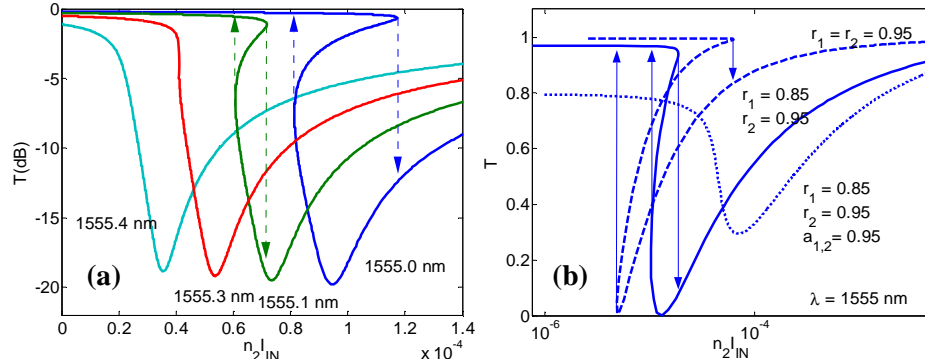


Fig. 11. T vs. $n_2 I_{IN}$ curves: (a) For various wavelengths, with $r_{1,2} = 0.85$, and $a_{1,2} = 0.99$. (b) For different asymmetries, as defined by the different (r_1, r_2) combinations. The dotted curve shows the loss of bistability when the upper ring is under the critical coupling condition.

The maximum extinction ratio achievable with an asymmetric Fano resonance is limited primarily by loss in the lower ring approximately as $\sim 1/(1-a)$. This can be shown by taking the maximum and minimum values of Eqs. (6) and (7). In the simplest case where the loss in the upper ring is negligible (i.e., $|T_2| = 1$), this gives:

$$ER_{\max}^{(T)} = \frac{T_{\max}}{T_{\min}} = \left(\frac{1+a_1}{1-a_1} \right)^2 \left(\frac{1-a_1 r_1^2}{1+a_1 r_1^2} \right)^2, ER_{\max}^{(D)} = \frac{D_{\max}}{D_{\min}} = \left(\frac{1+a_1 r_1^2}{1-a_1 r_1^2} \right)^2 \quad (10)$$

The calculated ER for both T and D, without assuming $|T_2| = 1$, are plotted as a function of a_1 in Fig. 12 for several values of r_1 (while r_2 is fixed). Note that the ER for T decreases, while that for D increases, with increasing r_1 . The Drop port (D) generally has a higher ER, but is exceeded by the Through port (T) when the loss is sufficiently small. For $a = 0.999$, the ER can be as high as 40dB. Such a low loss is possible, as demonstrated by some recent reports. First, a very high order multi-ring filters with very high Q resonators have been realized using low-loss Hydex material [1]. For polymer microring devices a thermal-reflow technique can be used to greatly reduce scattering loss [20]. Finally, an ultrahigh quality silicon-on-insulator (SOI) microring resonator with a Q of 139,000 has been reported [3]. All these suggest that it may be feasible to realize a high-ER switch using the two-ring device. The tradeoff, however, is that both extinction ratio and threshold power will be highly sensitive to wavelength, another consequence of the narrowness of the Fano resonance. Therefore, to increase the optical bandwidth one has to compromise the resonance sharpness and the switching threshold somewhat.

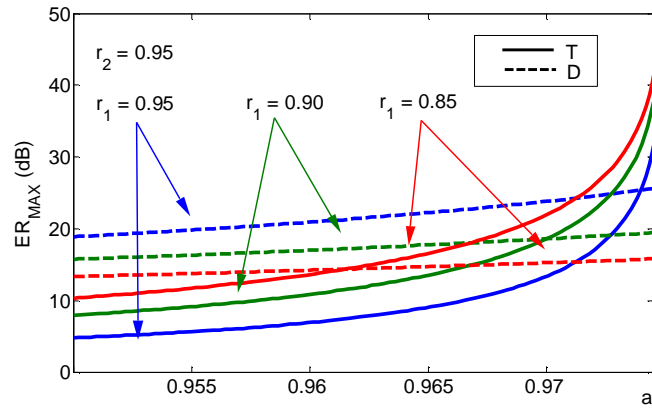


Fig. 12. Extinction ratio as a function of a_1 , for both T and D outputs, and for various values of r_1 .

Finally, we consider the dependence on the size of the ring and compare the one-ring and two-ring configurations. So far, in our calculations we have assumed the lower ring to have a radius of 15 μm . The two-ring device performance varies with the ring size in a way subtly different from the one-ring structure. The switching threshold in a one-cavity system is inversely proportional to the cavity size, in accordance with the inverse relation between the resonance linewidth and the cavity size. This rule applies also to REMZI. In the two-ring structure, the resonance broadening has little effect on the slope of the Fano resonance (the effect is similar to that of varying r in Fig. 10), which means that the slope is relatively unchanged with cavity size. There are also more parameters (such as r_1 , r_2 , and γ) that can be used to optimize the performance. A comparison between the two cases, for various ring sizes (where 1x refers to 15 μm radius), is shown in Fig. 13. Note that a two-ring structure with smaller rings still has lower threshold than a one-ring configuration with a larger ring. This clearly shows that the two-ring devices generally have much better performance than the one-ring configuration, and are not constrained by the conventional size dependence. The switching threshold can be one order of magnitude smaller, while the ON transmission is higher giving a better modulation depth. This winning edge is due to a tunable, narrow and

highly asymmetric Fano resonance made possible by the field dynamics in a two-cavity structure.

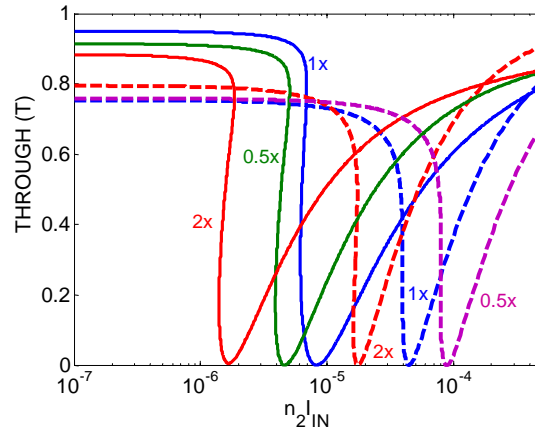


Fig. 13. The switching characteristics of the two-ring (solid) and one-ring (dashed) configurations with different cavity sizes. The cavity length is varied from 0.5 to 2 times the original length in both configurations, and the λ in each case is adjusted to achieve the lowest threshold. The coupling coefficient in both configurations is fixed, $r = r_2 = 0.95$. The (γ, r_1) for each of the two-ring cases is different, and from 0.5x to 2x, are given by (1.005, 0.8), (1.05, 0.85), and (1.05, 0.75), respectively.

5. Conclusion

We have considered the switching performance of three different ring configurations. We show that high extinction ratio (> 10 dB), large modulation depth (~ 1), and low switching threshold ($n_2 I_{IN} \sim 10^{-5}$) over a signal bandwidth of 0.1 nm (10 GHz) can be simultaneously achieved by both the ring-enhanced MZI and the simple two-ring configuration. In contrast, for the one-ring case, both one-bus and two-bus, although they can achieve a similar ER, they inevitably fare poorer in terms of modulation depth, switching threshold and signal bandwidth.

In both cases, the switching mechanism is fundamentally based on a tailorable asymmetric Fano resonance which can be significantly sharper than the symmetric ring resonance. The Fano resonance arises from the interference between two pathways. In the two-ring case, the interference causes a splitting of the resonance; the amount of splitting and the shapes of the resonances can be tuned by varying the physical parameters of the rings and their coupling. In the case of REMZI, the Fano resonance arises from the interference between the resonant phase of the ring and the static phase bias in the MZI. The sharpness and the shape asymmetry of the Fano resonance contribute, respectively, to the low switching threshold and the high extinction ratio of the optical switches. The ER may be maximized by minimizing the ring loss, and by optimizing the coupling between the ring and the bus waveguides. In general, the switching threshold for the two-ring device and the REMZI may be one to two orders of magnitude smaller than the one-ring configurations. In practical terms, assuming a polymer material such as the PTS whose Kerr index is $n_2 = 5 \times 10^{-12}$ cm²/W [19], and a waveguide with a cross section area of 1 μm^2 , $n_2 I_{IN} \sim 10^{-6}$ implies a threshold power of 2mW. This theoretical value is 30x smaller compared with the theoretical result of Dumeige which is based on the dual-bus one-ring structure [7]. In reality, one must also consider two-photon absorption and free carrier refraction, which will further reduce the switching threshold [21].

We like to acknowledge the partial support of a Singapore Ministry of Education research grant (RG12/03).